

IOWA STATE UNIVERSITY

Institute for Physical Research and Technology

AD-A257 292



September 23, 1992

Center for
Nondestructive Evaluation
Applied Sciences Complex II
1915 Scholl Road
Ames, Iowa 50011
515 294-8152
FAX 515 294-7771

①

Robert J. Silverman
Administrative Grants Officer
Department of the Navy
Office of Naval Research
University of Washington
410 University District Building
1107 N. E. 45th Street
Seattle, WA 98105-4631

rots
Eleanor Dizon is checking on

RE: 1425:RJS:ead
N00014-90-J-1696

S DTIC ELECTE D
A
OCT 09 1992

Dear Mr. Silverman:

Enclosed is a copy of a letter and reports which were submitted in April of this year as a final report on the above stated project. R. Bruce Thompson received a "Tracer" from you again requesting the final report. On the second request for a final report, an address in Alexandria, Virginia was highlighted as to the submittal address. At this time, I'm sending the report to both you and the Virginia address.

In trying to figure out what happened to the original report sent in April, I noticed that the grant numbers on our report and the number on your request letter differ. Apparently the number we used related to the original grant that was set up with the University of Illinois and was not changed on our reports to the more recent contract directly with ONR.

Please contact me immediately if you need further information regarding this final report.

Sincerely,

Libby Bilyeu
Libby Bilyeu
Program Assistant

Enclosures

This document has been approved
for public release and sale; its
distribution is unlimited.

IOWA STATE UNIVERSITY
Institute for Physical Research and Technology

Center for
Nondestructive Evaluation
Applied Sciences Complex II
1915 Scholl Road
Ames, Iowa 50011
515 294-8152
FAX 515 294-7771

April 10, 1992

Robert J. Silverman
Administrative Grants Officer
Department of the Navy
Office of Naval Research
University of Washington
410 University District Building
1107 N. E. 45th Street
Seattle, WA 98105-4631

Dear Mr. Silverman:

Enclosed is information being submitted in response to a final report for Grant N00014-90-J-1698. The quarterly report was written as a review of the whole project. David Hsu also made a presentation at the ONR review in Annapolis in September of 1991. His talk covered all results obtained by the ISU group.

Also enclosed is a copy of a paper presented by R. Bruce Thompson at the Winter meeting of ASME in December, 1991. This paper also covered the results for the entire project.

Please contact me if you feel more information is needed in regard to the final report.

Sincerely,



Libby Bilyeu
Program Assistant

Enclosures

NDE for Thick Section Composites

Accession For	
NTIS CRA&I	<input checked="" type="checkbox"/>
DTIC TAB	<input type="checkbox"/>
Unannounced	<input type="checkbox"/>
Justification	
By _____	
Distribution/	
Availability	
Dist	
A-1	

ONR Quarterly Report
July 1 - September 30, 1991
Contract #N00014-86-K-0799

Iowa State University
Center for NDE
Applied Science Complex II
1915 Scholl Road
Ames, IA 50011

DTIC QUALITY INSPECTED I

Dist A per telecon Ms. E. Dixon
Office of Naval Research
University of Washington
410 University Dist Bldg
1107 N.E. 45th Street
Seattle, Washington 98105-4631
10-9-92 CG

92 10 7 098

425610
92-26747
2098

Table of Contents

	<u>Page Number</u>
- Task 1: Elastic Properties of Thick Composites..... Emmanuel P. Papadakis and Yu Min Tsai	1
Task 2: Defect Characterization..... David K. Hsu	6
Task 3: Discrete Defect Characterization..... Michael S. Hughes, David K. Hsu, and David K. Holger	9

TASK 1: ELASTIC PROPERTIES OF THICK COMPOSITES

REPORT PERIOD: July 1 - September 30, 1991

PRINCIPAL INVESTIGATOR: Emmanuel P. Papadakis

INVESTIGATOR: Yu-Min Tsai

STUDENT: Thadd Patton (through April, 1991)

OBJECTIVE:

To measure and report on the elastic moduli of thick, graphite-epoxy, filament-wound composites.

The purpose of this work is to permit the calculation of allowed elastic wave modes and directions for nondestructive evaluation of thick composites. In addition, the anisotropic elastic moduli so obtained will contain important information about the microstructure of the material and the vibration characteristics of structures made from it. As the material has been found to be highly anisotropic, it is expected that ultrasonic interrogation to find flaws will be complicated. To calculate the wave propagation phenomena which may be useful or detrimental, it is necessary to measure the elastic moduli of the material.

APPROACH:

The approach is to investigate the possibility of using an array of static as well as dynamic elastic measurement methods to determine the elastic moduli of the materials in the symmetry and configuration of the composites. The parts of greatest interest are cylinders with the symmetry axes defined as 1 = axial, 2 = hoop, and 3 = radial. With the theoretical expressions for the measurable variables available, it will be possible to pick a feasible set of measurements from which to calculate the nine elastic moduli of the materials.

Having a complete array of theories is of importance from two points of view:

(1) The contracting agency wishes to be able to determine the moduli by using uncut right circular cylinders as manufactured rather than having to cut special specimens for laboratory measurement. To date, the measurements have been made on specimens cut analogous to crystals of similar local symmetry. One full-size cylinder has been obtained to continue the work, and the theories are necessary for the interpretation of measurements made in this geometry.

(2) Certain deformations may prove particularly advantageous for flaw detection. These can only be identified and fully exploited with a proper theoretical foundation.

The array of theories and techniques can be subdivided as follows to provide specific approaches:

- A. Ultrasonic Traveling Bulk Waves
 - 1. Normal Incidence
 - 2. Oblique Incidence
 - 3. Surface Excitation by Line Contact
 - 4. Surface Excitation by Oblique Immersion
- B. Ultrasonic Traveling Surface Waves
- C. Ultrasonic Traveling Lamb Waves
- D. Body Vibrations
- E. Static Stress-Strain

Progress on these techniques will be reported in the next section. Both theory and experiment will be mentioned.

PROGRESS TO DATE:

A. General

Theoretical work was carried on to find methodologies for measuring the elastic moduli of thick composites in the form of uncut right circular cylinders. Orthorhombic point group symmetry is assumed.

B. Theoretical

The dependence of the Lamb wave speeds on the anisotropic material constants in the relatively low frequency range was reported in the last quarter. The antisymmetrical frequency equation was written in a polynomial form. In this range of relatively low frequency, the wave speeds of the antisymmetrical Lamb waves were reported to be significantly different from those for the symmetrical Lamb waves. In the investigation of the symmetrical Lamb waves in this quarter, an orthotropic plate is assumed to have an arbitrary thickness of $2H$ in the principal y -direction. A plane harmonic wave with frequency ω is propagating in the other principal z -direction. Solution for the equations of motion are obtained and the stress-free surface conditions of the plate are satisfied.

A closed-form expression for the frequency equation for the symmetrical Lamb waves has been obtained. The half plate thickness H is small, compared to the wave length Λ in the low frequency range. The symmetrical frequency equation is investigated for a small value of the parameter $\lambda = 2\pi H/\Lambda$. The first-order approximation of the frequency equation yields the following plate wave speed c :

$$c = (\alpha - \delta^2/\beta)^{1/2} c_2$$
$$\alpha = c_{33}/c_{44}, \quad \beta = c_{22}/c_{44}$$
$$\delta = c_{23}/c_{44}, \quad c_2 = (c_{44}/\rho)^{1/2}$$

Second-order approximations of the symmetrical frequency equation gives the following expression in terms of the wave speed ratio $r = c^2/c_2^2$:

$$\beta(\alpha - r) + \delta(r + \delta) + \delta b$$
$$+ \lambda^2 \{ [\beta(\alpha - r) + \delta(r + \delta)]b/\beta + \beta\delta A + (r + \delta)(\alpha - \delta) \} / 6$$
$$- \lambda^2(\alpha - r)r(1 + \delta)/2 = 0$$
$$b = 1 - r + \beta(\alpha - r) - (1 + \delta)^2,$$
$$A = [2b^2 + 4\beta(\alpha - r)(r - 1)]/4\beta^2$$
$$+ (\alpha - r)(1 - r)/\beta$$

The above second-order equation can be seen as a quadratic equation for $r = c^2/c_2^2$ in terms of the ratios of material constants and the parameter $\lambda = 2\pi H/\Lambda$. The speed c of the symmetrical Lamb wave can be determined from the roots of the quadratic equation. The results reveal the parabolic dependence of the symmetrical Lamb wave speed on the ratio of the half plate thickness H to the wave length Λ and the anisotropic material constants.

The above results for Lamb waves in y (thickness) and z (propagation directions) coordinates can be approximately applied to ultrasonic waves propagating in a hollow composite cylinder when the wall thickness is small with respect to a wavelength. In the nomenclature used in experiments, axial, circumferential (hoop) and radial directions of a composite cylinder are respectively indicated as 1, 2 and 3 coordinates. For a symmetrical Lamb wave propagating in the axial direction of a cylinder with wall thickness $2H$, the above results apply if the material constants ratios take the following forms:

$$\alpha = c_{11}/c_{33}, \quad \beta = c_{33}/c_{55}, \quad \delta = c_{13}/c_{35}$$

$$\text{and } c_2 = (c_{55}/\rho)^{1/2}.$$

For the case of symmetrical Lamb waves traveling around the circumference, the ratios are

$$\alpha = c_{22}/c_{44}, \quad \beta = c_{33}/c_{44}, \quad \delta = c_{23}/c_{44}$$

$$\text{and } c_2 = (c_{44}/\rho)^{1/2}$$

Four elastic constants are involved for each case of ultrasonic wave propagation.

C. Summary

1. Theory

(a) Ultrasonic traveling bulk waves. Equations for the velocities of ultrasonic traveling bulk waves have been derived for orthorhombic materials in forms to yield values for the elastic moduli. With respect to the surfaces normal to the three principal axes of the material, the various sets of equations are valid for normal incidence, oblique incidence, surface excitation by line contact, and surface excitation by oblique immersion. The theory of slowness surfaces has been worked out for the oblique directions.

(b) Ultrasonic traveling surface waves. Equations for the velocities of ultrasonic traveling surface waves have been derived for orthorhombic materials in forms to yield values for the elastic moduli in certain combinations as simultaneous equations. Use of some velocities of bulk waves in available (uncut) bulk directions facilitate the use of the surface wave equations.

(c) Ultrasonic traveling Lamb waves. Equations for the velocities of symmetrical and antisymmetrical traveling Lamb waves have been derived for orthorhombic materials in forms to yield values for the elastic moduli in certain combinations as simultaneous equations. Use of some velocities of bulk waves in available (uncut) bulk directions facilitates the use of the Lamb wave equations.

(d) Body vibrations. While constitutive equations have not been worked out, it is expected that certain modes will act like superpositions of Lamb waves in eigenvalue problems.

(e) Static stress-strain. This effort was not undertaken because it appeared to be covered by work at the David Taylor Research Center.

2. Experimental

(a) Bulk waves in cut specimens. The measurements using bulk waves in cut specimens have been completely successful. The velocities of ultrasonic longitudinal and shear waves have been measured by through-transmission. Specimens had two basic shapes: rectangular parallelepipeds and parallelepipeds with one pair of parallel faces cut at an oblique angle of 45°. The propagation vectors could then lie along each principal axis and at 45° between each pair of principal axes.

A complete set of measurements was made on experimental rocket casing material from Hercules. Because of the high anisotropy resulting in large differences between the 3-direction (radial, through the thickness) and the other two quite similar directions due to the lay-up (1 = axial, 2 = hoop), the slowness surface theory had to be applied for the 1-3 plane and the 2-3 plane to find the exit point of the Poynting vector in through transmission. This was done successfully. The matrix of elastic moduli is recapitulated here in units of giga-Pascals (GPa):

Hercules Material (-33, 90, 33 combinations)

$$\begin{pmatrix} 47.3 & 28.1 & 7.86 & 0 & 0 & 0 \\ 28.1 & 36.6 & 3.75 & 0 & 0 & 0 \\ 7.86 & 3.75 & 9.54 & 0 & 0 & 0 \\ 0 & 0 & 0 & 2.90 & 0 & 0 \\ 0 & 0 & 0 & 0 & 3.44 & 0 \\ 0 & 0 & 0 & 0 & 0 & 18.2 \end{pmatrix}$$

The "softness" of the material between the layers of plies is seen in the low values of

(a) c_{33} versus c_{11} and c_{22} ,

(b) c_{44} and c_{55} versus c_{66} ,

and

(c) c_{13} and c_{23} versus c_{12} .

All wound thick composites are expected to show this behavior. It is expected that 0, 90 lay-ups will have lower values of c_{12} and c_{66} than lay-ups at -45, 0, 45, 90 or -33, +33, 90 because of the lack of any triangular cross-stiffening in the 1-2 plane.

Because of the small thickness of the Navy cylinders, it was not possible to make a complete set of measurements. Miniaturization of the probes and fixtures would have been necessary but was not possible within the funding. The values of c_{13} and c_{23} were not determined in the Navy experimental material. Other values are recapitulated here in units of GPa.

Navy Material

Constant	Lay-Up	
	[90 ₄ /0 ₂] ₁₃ 90 ₃	[90 ₂ /0 ₂ /+45 ₂ /-45 ₂] ₁₀ 90
c_{11}	71.9	64.3
c_{22}	127.2	70.6
c_{33}	14.1	14.2
c_{44}	5.46	4.56
c_{55}	4.36	4.98
c_{66}	8.11	20.9
c_{12}	11.5	24.9
c_{13}	N/A	N/A
c_{23}	N/A	N/A

The prediction of the affect of stiffening by the $\pm 45^\circ$ plies can be seen to be correct, as c_{12} and c_{66} are caused to double by adding these plies. It will be seen that c_{22} is high in the [90₄/0₂]₁₃90₃ configuration because of the larger number of windings in the 90 ° orientation. It is expected that c_{13} and c_{23} will be no more than 25% of c_{12} in either case.

A slab made by hand lay-up at CNDE in the [0₃/90]_N configuration was also tested and found to give good results including c_{13} and c_{23} when the slowness surfaces were taken into account. The moduli of this material are given here in GPa.

CNDE Hand Lay-Up [0₃/90]_N

Constant	Value
c_{11}	134.4
c_{22}	50.9
c_{33}	14.4
c_{44}	4.23
c_{55}	5.64
c_{66}	6.98
c_{12}	11.9
c_{13}	17.0
c_{23}	12.1

Here, the lack of cross-ply stiffening leaves c_{12} and c_{66} low. The value of c_{11} is high because of the larger number of plies at 0°.

Experiments with surface excitation of bulk waves and surface waves met with mixed results. The head wave at the bulk velocity generally agreed with the actual bulk wave. Surface waves often gave complex numbers as moduli or moduli which were too large to be plausible. Further work is needed. Future experiments should include spatially periodic transducers to match wavelengths and frequencies for expected velocities. The water tank methods should be followed up, also.

No experimentation was carried out on Lamb waves or on static stress.

TASK 2: DEFECT CHARACTERIZATION

REPORT PERIOD: July 1, 1991 - September 30, 1991

PRINCIPAL INVESTIGATOR: David K. Hsu

STUDENT: Ali Minachi

OBJECTIVE:

To develop ultrasonic methods for evaluating defects and elastic properties of thick composites.

ACHIEVEMENTS OF THIS TASK:

This was the last quarter of the ONR/URI project. The main activities in this concluding quarter included reporting research results obtained over the last three years to ONR at the program review meeting held in Annapolis on September 12 and 13, 1991; reporting recent results on in-situ elastic constant measurement of thick composites in the Review of Progress in QNDE conference held in Brunswick, Maine; and writing a paper for the QNDE proceedings.

As a last report, it serves useful purposes to look back and review what had been done, what are the significance of the results, what applications the results have, and what should be done next. For this reason, a brief review is given below for the accomplishments of Task 2.

I. Ultrasonic evaluation of porosity in thick composites

The presence and severity of porosity in a thick composite depend on the manufacturing process and may be a quality reliability concern in some applications. In this work, methods developed previously for thin composites were tested in filament-wound, thick composites (1.4"). In previous work a linear relationship between the porosity volume fraction and the attenuation slope (i.e., derivative of the attenuation with respect to frequency) has worked reasonably well. The constant of proportionality, however, depends on the pore morphology. The difficulty of quantifying porosity in thick filament-wound rocket motor case, however, was that the pore size and shape varied greatly and were location dependent. For example, ultrasonic attenuation measurements at a particular point predicted that the void content was from 2.6% to 3.6% if the voids were assumed to be flat, long cylinders; or 5.2% to 7.2% if the voids were assumed to be spherical. Acid digestion of a piece adjacent to the measurement location yielded a void content of approximately 4.4%. The void content from acid digestion fell between the two extremes and was closer to the flat, long void assumption. For future work, porosity parameters (such as void size and shape distribution) should be determined for the material system of interest. These parameters would help the establishment of an empirical but useful relationship between void content and the measured ultrasonic attenuation.

II. Sizing of circular delaminations using beam model

When a transducer is scanned over a circular flaw such as a delamination, the way the flaw echo amplitude varies with distance contains size information. Since the thick composite is elastically anisotropic, the sizing of flaws is more difficult than in an isotropic solid. A method was developed in this task in which the flaw size was determined iteratively by seeking the best agreement between the experimental data and the computed variation of flaw echo amplitude with lateral distance. The computation uses the Gauss-Hermite model for the ultrasonic beam propagation and takes into account the transducer size, the frequency, the flaw depth, and the elastic anisotropy. The last item was accounted for based on the slowness surfaces of the material system of interest.

III. Acousto-ultrasonic effect in thick components

In the development of NDE methods for thick section composite structures, one has to keep in mind that eventually in-situ and one-sided techniques must be developed for the inspection of large structures. The inspection technique needs to be one-sided because the back side of large composite structures are normally inaccessible. The method needs to be in-situ because it is necessary to evaluate the material properties and defect conditions as a function of location on large composite structures. Toward this goal, an effort was made in this task to gain a physical and quantitative understanding of obliquely reflected ultrasonic modes in an elastically anisotropic thick

composite. The configuration of interest was the so-called "acousto-ultrasonic" setup where two transducers were coupled to the same surface of the thick structure, one serving as the transmitter and the other as the receiver.

In this work, it was found that the acousto-ultrasonic signals in thick composites consisted of many types of waves. These waves included obliquely reflected, quasi-longitudinal and quasi-transverse bulk waves, surface skimming longitudinal waves, and surface waves. In a pulsed measurement the echoes associated with these modes can be temporally resolved due to the large thickness of the part. Since the composite is anisotropic, the energy vector of the quasi-modes do not coincide with the phase velocity direction. The model used in analyzing the various modes in the acousto-ultrasonic signals was based on the slowness surfaces of the composite under study. The slowness surfaces were computed using the elastic constants of the composite. The times-of-flight of the various modes were calculated using the slowness surfaces and the fact that the group velocity direction (i.e., the direction in which the energy propagates) was always perpendicular to the local curvature of the slowness surface.

Using a unidirectional graphite/epoxy thick laminate, experiments were performed to measure the time-of-flight of the various modes of the acousto-ultrasonic signals, including mode-converted echoes and multiple echoes. The measured results were successfully interpreted using the slowness surfaces and the agreement was excellent. This formed the basis for the inverse problem: the nondestructive in-situ measurement of elastic constants of thick composite structures with only one side access.

IV. In-situ one-sided determination of elastic constants

For a given composite, three elastic constants can be determined immediately using one normal incidence longitudinal wave and two normal incidence shear modes. The remaining elastic constants may be determined from the times-of-flight of acousto-ultrasonic signals in an iterative manner. Since there are many modes (for example, there are QL \rightarrow QL, QL \rightarrow QSV, QSV \rightarrow QSV, SH \rightarrow SH, etc., in a unidirectional composite,) the inverse problem is overspecified. The exact iteration procedures depend on the elastic symmetry of the composite, but the approach may be illustrated in the unidirectional case, as follows.

A unidirectional composite has hexagonal symmetry and five independent elastic stiffness constants. With the fibers running in the x-direction, these constants are C_{11} , C_{22} , C_{44} , C_{55} , and C_{12} . For a plate of unidirectional composite with fibers lying in the plane, the three constants C_{22} , C_{44} and C_{55} are determined using normal incidence contact mode ultrasonic velocity measurements. The remaining two constants C_{11} and C_{12} are determined iteratively using the times-of-flight of Acousto-ultrasonic echoes. Among the many echoes in an acousto-ultrasonic RF waveform, the echo with the smallest time-of-flight (which is not a surface wave) is the QL \rightarrow QL echo. The surface wave echo is easily identified and ruled out because its time-of-flight extrapolates through zero at zero separation of the transducers. By assuming some initial guess of the two unknown constants, the slowness surfaces, and hence the times-of-flight of the QL \rightarrow QL echo, are calculated. The calculated and measured times-of-flight are compared, and their difference is minimized by iteratively changing the values of the two constants. When the best agreement is found, the last values of the two constants used are taken to be the values being sought.

In practice, there are a number of experimental difficulties and systematic errors to be dealt with. For example, the measured times-of-flight contain errors due to the finite (nonzero) width of the pulse and due to the finite size of the transducers. These effects tend to introduce a constant error in the measured times. Therefore, the measured times are varied by an additive constant during the iteration process until the discrepancy between experiment and theory is the smallest. This method of eliminating the systematic error seems to stabilize the inversion process and produce good results. In the 1" thick unidirectional composite of graphite/epoxy, the values of C_{11} and C_{12} obtained from the iteration process are respectively 124 ± 3 GPa and 7.7 ± 0.1 GPa. Compared to values obtained by doing ultrasonic velocity measurements on cut pieces, the determination of C_{11} was quite accurate (to within a few percent), but the accuracy for C_{12} was somewhat lower (to within 12% or so.) Accurate determination of C_{12} is very difficult because the dispersion equations are such that a change in C_{12} affects the time-of-flight of the various modes only slightly. To improve the sensitivity, data should be taken with large transducer separation distances (not difficult to do on thick composites) and perhaps to use a combination of modes in the iteration process.

CONCLUDING REMARKS

Considerable information has been obtained in this task of the ONR/URI project. In particular, a foundation has been established for the nondestructive evaluation of elastic properties of thick composites in the in-situ, single-sided mode. It would be fruitful to extend the technique to other layups such as 0/90 or quasi-isotropic structures and to filament-wound structures. In the area of flaw sizing and characterization, progress has been made in this task toward the development of a model-based flaw sizing method that takes into account the effects of frequency, transducer size, beam spreading and material anisotropy. Future development should merge with the effort to size and image flaws using the synthetic aperture focusing technique (SAFT.) Other flaw types such as porosity and ply waviness are also important in thick composites and should be addressed from both an experimental and analysis approach. In conclusion, the NDE of thick composites is indispensable in the manufacture and development of large composite structures. The NDE effort must be viewed in the broader sense to include nondestructive evaluation of material properties and nondestructive characterization of defects and flaws.

TASK 3: DISCRETE DEFECT CHARACTERIZATION

REPORT PERIOD: July 1 - September 30, 1991

PRINCIPAL INVESTIGATORS: Michael S. Hughes, David K. Hsu

OBJECTIVE:

SAFT reconstruction has been employed for the analysis of NDT data for over ten years [1-7]. Excellent results have been obtained in both metals and biological media [1-7]. In these materials the propagating medium may be modeled to first approximation as lossless and isotropic. It is obvious however, that these assumptions are less likely to provide a good approximation to composite materials. In this report we describe tests performed on various types of composite layups in order to test the degree to which the lossless-isotropic model succeeds or fails. Our primary goal is a quantitative investigation of the image artifacts introduced into the SAFT reconstruction by material anisotropy.

APPROACH:

Data were acquired in immersion mode using a 5.0 MHz center frequency, 4.0 inch focal length, broadband, 1.0 inch dia. transducer. The transducer was focussed on the surface of the sample by maximizing the amplitude of the frontwall echo. As Seydel has pointed out this is not necessary for SAFT imaging although it is conventional [1]. The transducer was connected to a conventional ultrasonic pulse/echo unit whose output was digitized at 100 MHz sampling rate in a digital sampling oscilloscope and transferred into a computer for storage and later off-line analysis. All samples were scanned in a line with spacing between adjacent points kept smaller than one half of a wavelength at the center frequency 5.0 MHz. At each point, 200 rf traces were digitized and averaged to obtain improved signal to noise ratio for the stored data.

These traces were analyzed off-line to produce both B-Scan images and SAFT reconstructions according to the algorithm described by Seydel. Our algorithm is a modified version of an implementation developed by Battelle Pacific Northwest Laboratory and provided in the form of C source-code. Our modifications have been aimed at improvements in execution time, reduction in computer memory requirements, portability, and easy linking to routines which make use of material elastic constants to calculate slowness surfaces to be used for later anisotropy corrections. The first two requirements have been met well enough to permit all of the SAFT reconstructions shown here to be run in two minutes on a Apple Mac II personal computer which is certainly not a powerful number crunching platform. Analysis proceeds as follows. A waveform is read into memory from hard disk and the average value of that waveform within a user defined interval is computed and subtracted from each voltage in that waveform. This is done in order to remove D.C. offsets which can corrupt the final image. Next, the waveform is gated so that only a subset of the recorded trace is used in the reconstruction. This gate is also user definable and is necessary in order to exclude front and backwall echoes which would otherwise saturate the reconstructed image (eight bit dynamic range for all figures in this paper). Finally, the remaining rf data points are added into the appropriate pixels in the reconstructed image according to the time-shift formulas described by Seydel. These shifts include a user defined offset identifying the time position of the frontwall reflection which it is necessary to include in order to obtain absolute depth information from the reconstructed image (again described by Seydel). After this is done the next trace is read into memory and the process repeated until all stored traces have been exhausted.

PROGRESS TO DATE:

Our study was based on data acquired from three samples. The first two, one made of plexiglas™ and one made of [0,90] graphite/epoxy composite (orthorhombic symmetry) were designed to test image distortion introduced for the type of material anisotropy exhibited by [0,90] layup. In order to do this, five flaws, an elongated flat bottom slot aligned parallel to the long axis of the sample, a flat bottom slot across the sample, a side drilled hole, and two flat bottom holes were identically machined into both blocks as shown in Figure 1.

Figures 2a and 2b present data for the plexiglas™ sample. Figure 2a contains the raw data presented in B-Scan format (each rf A-line contains 2048 points 0.02μs apart). The downward concavity of the defects shown in the B-Scan is the expected result and arises from the increased path length traversed by the insonifying beam as it sweeps over the defects. All defects are evident in the image at depths that lie within 1% of the values shown in Fig. 1 (using a longitudinal velocity of 2240 m/s). However, the widths of the defects are clearly exaggerated. Figure 2b is a SAFT reconstruction of the data shown in Fig. 2a. All depths are correct to within 1%. In addition, the widths of the defects are noticeably smaller than those on the B-Scan image, as they should be, and agree to within 5% of the actual values shown in Fig. 1.

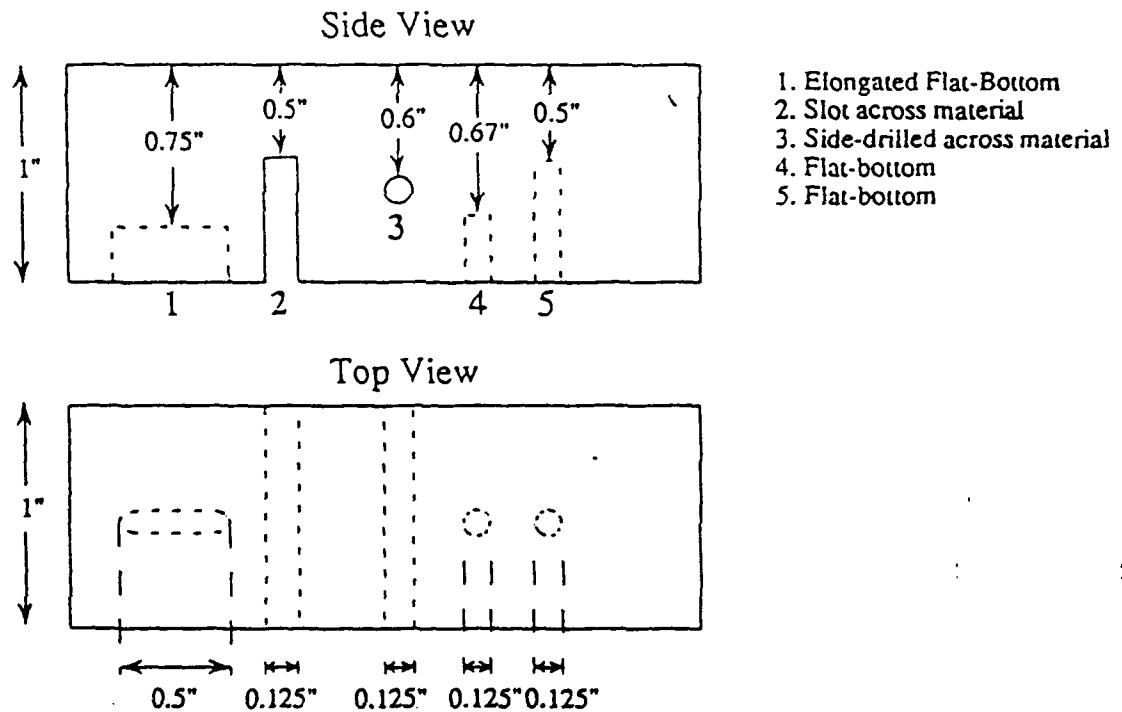
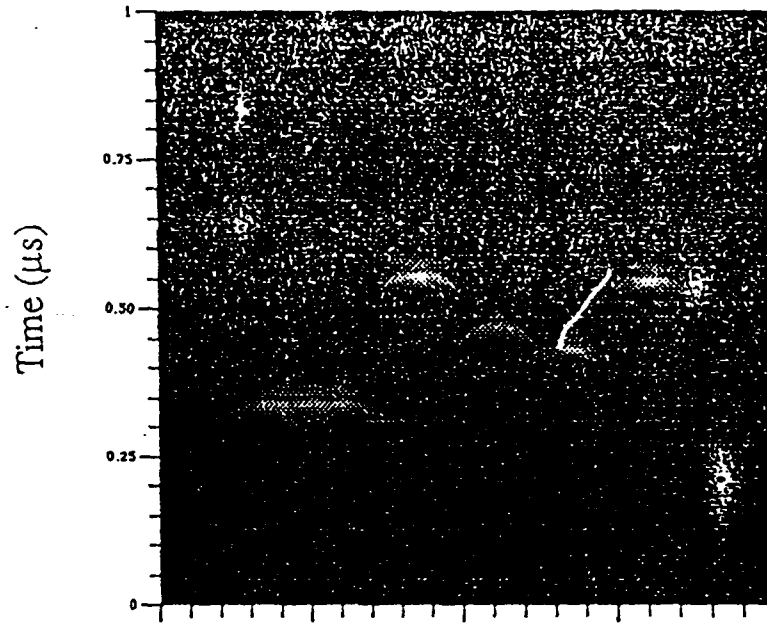


Figure 1. Flaw geometry used to determine the effect of anisotropy in a [0,90] graphite/epoxy layup on the accuracy of the SAFT reconstruction algorithm.



SAFT Image for Plexiglas™ Sample

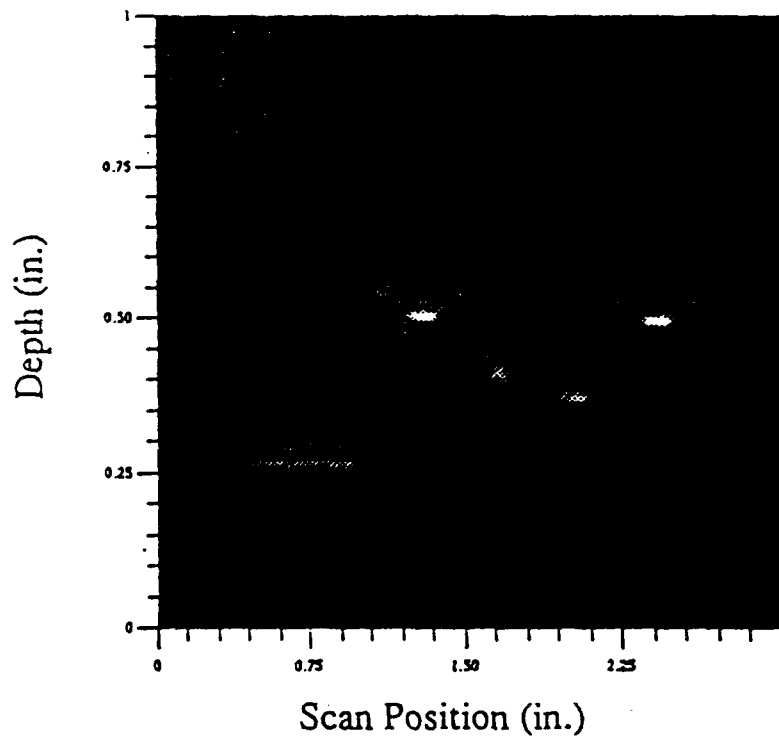
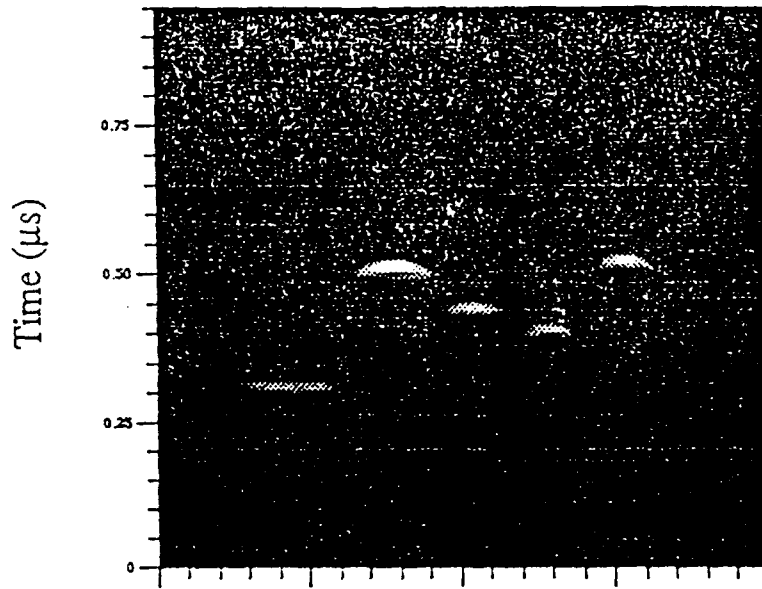
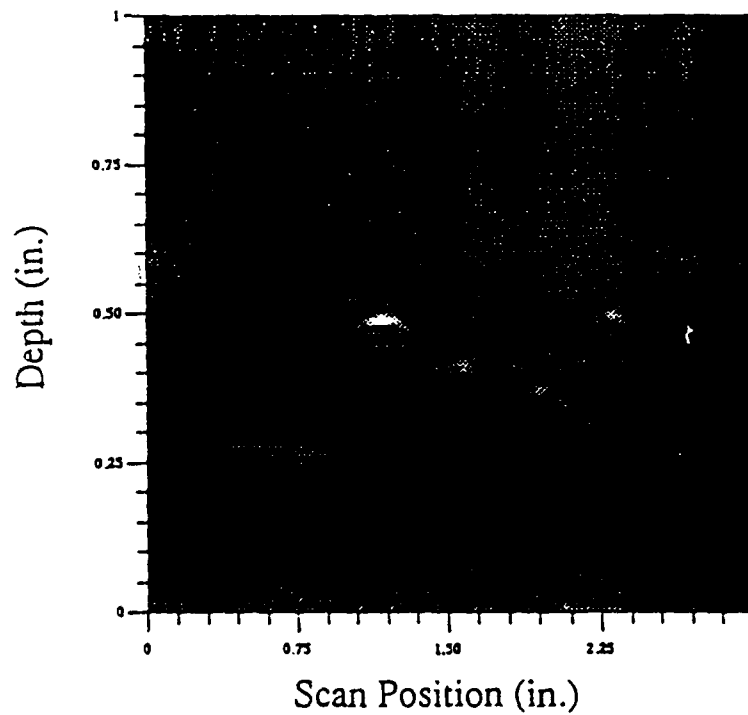


Figure 2. Comparison of B-Scan and SAFT reconstruction for line scan data taken from a plexiglas™ sample having the flaws shown in Fig. 1. Top panel A the B-Scan showing exaggerated flaw widths. Bottom panel B SAFT reconstruction using same data; flaw widths are now within 5% of actual values.



SAFT Image for
Plexiglas Sample



SAFT Image for
[0°,90°] GR/EPX Sample

Figure 3. Comparison of B-Scan and SAFT reconstruction for line scan data taken from a [0,90] layup graphite/epoxy composite sample having the flaws shown in Fig. 1. Top panel A the B-Scan showing exaggerated flaw widths. Bottom panel B SAFT reconstruction using same data; flaw widths are now within 5% of actual values.

Figures 3a and 3b present data for the composite sample. The downward concavity of the defects shown in the B-Scan is again apparent as are all defects; from the image their depths are all found to lie within 1% of the values shown in Fig. 1 (using a velocity of 2740 m/s and the fact that each rf A-line contains 2048 points 0.02 μ s apart). However, as in Fig. 2a, the widths of the defects are exaggerated. The reconstructed SAFT image is shown in Fig. 3b. Once again, all depths are correct to within 1%. Furthermore, the widths of the defects are noticeably smaller, as they should be. In fact, they differ from the actual values by less than 5% (using FWHM criteria), which is surprising since the material is anisotropic and our reconstruction algorithm does not yet account for this effect. We speculate that the [0,90] layup may approximate an isotropic medium well enough to permit this level of agreement at the limited aperture used in the reconstruction. Some differences from the isotropic case, however, are evident if the data shown in Figs. 2a and 3a are plotted as wire plots (not shown); in this form the indications for the flat bottom slots show a greater degree of flattening in the isotropic case than in the anisotropic case. This may be due to the effects of anisotropy, which tend to defocus the synthetic aperture.

The fact that the anisotropy did not degrade the sizing accuracy is a somewhat surprising result and is presently being examined more closely using uniaxial samples (hexagonal symmetry). This sample comprises the third used in our study and is shown in Figure 4. This sample which is 192 plies thick has nominally identical flaws (teflon strips 0.1875 in. wide included between the 32nd and 33rd plies) aligned in orthogonal directions relative to the fiber direction as shown in the figure. For the purposes of our study the sample was insonified from the stepped side (the "bottom" side in Fig. 4) so that the dependence of anisotropic effects on depth could be tested.

The results of a one inch line scan (0.005" steps over a total length of 1.0") of the strips in the thin (0.4") step are shown in Figures 5a and 5b. The top panel, Fig. 5a, shows that SAFT reconstruction obtained for the 0.1875" teflon strip (correspondingly labeled in Fig. 4) obtained by scanning the transducer parallel to the fibers. Quantitative measurements taken from the image (FWHM criteria) show that the measured width is within 5% of the nominal value. The SAFT reconstruction for data obtained scanning perpendicular to the fibers is shown in Fig. 5b; the FWHM width in this case is also within 5% of nominal.

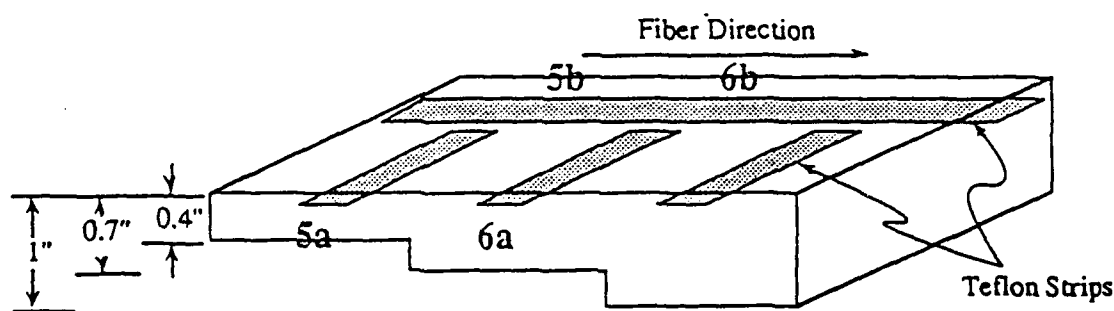


Figure 4. Uniaxial graphite/epoxy composite used to determine effect of anisotropy on SAFT reconstruction algorithm.

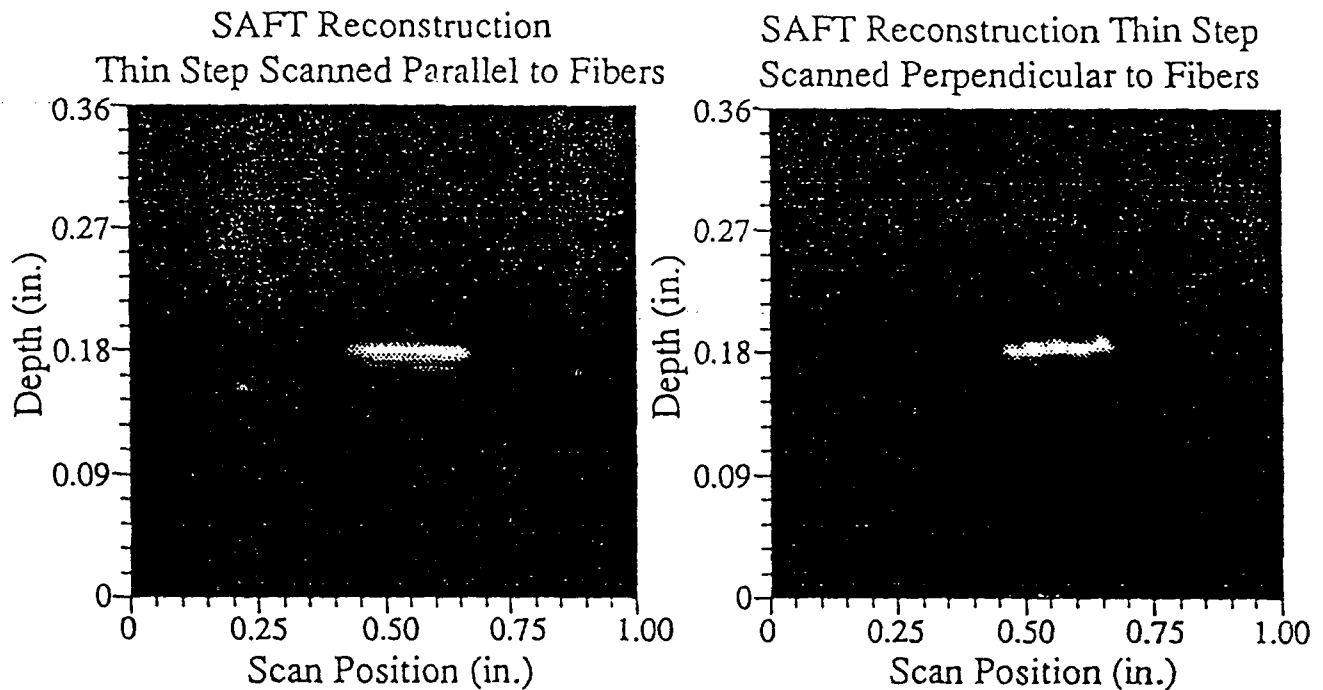


Figure 5. SAFT reconstructions of teflon strips from the thin step of the sample shown in Fig. 4. Inset panels show the scan direction relative to the fiber orientation i.e. the orientation of the synthetic aperture relative to the fiber direction. Left panel A: synthetic aperture aligned parallel to fibers. Right panel B: synthetic aperture aligned perpendicular to fibers.

Data obtained from the middle step is shown in Figure 6. In this case the relative differences in reconstructed flaw widths are more dramatic. This is consistent with the increased effects of anisotropy arising from the longer path lengths traversed by the insonifying beams. In panel A we see the reconstruction resulting when the synthetic aperture is aligned parallel to the fiber direction. In this case the estimated flaw width is nearly twice as large as it should be. Panel B shows the case where the synthetic aperture is aligned perpendicular to the fiber direction. In this case the effects of anisotropy are expected to be smaller and, indeed, the estimated flaw width from the figure is within 5% of nominal value. Some of the variations shown above may be due to real variations in the width of the teflon strip arising from the fabrication process. In this regard, the results presented so far must be viewed as preliminary. Further work using flat bottom slots, like those used in the [0,90] study are now under way.

CONCLUSIONS:

Several examples of demonstrating the impact of material anisotropy on the SAFT reconstruction algorithm have been shown. These point out the need to incorporate the effects of

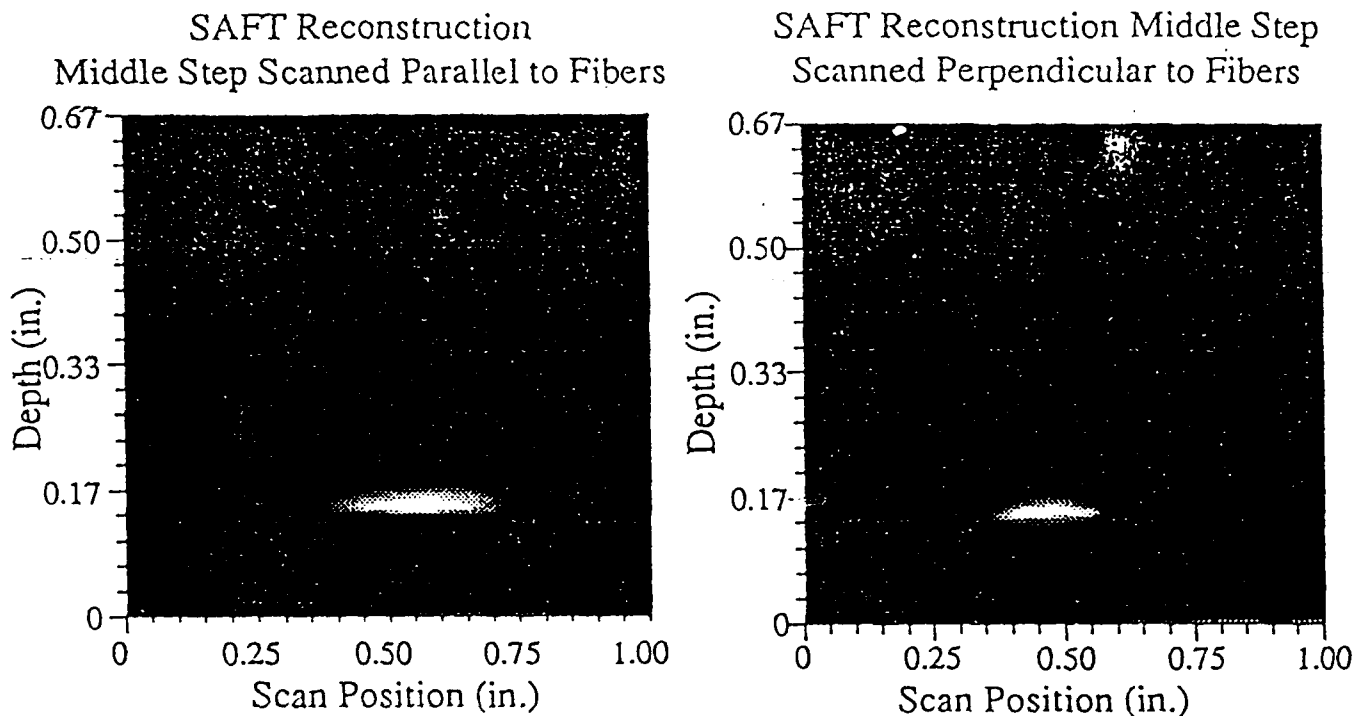


Figure 6. SAFT reconstructions of teflon strips from the middle step of the sample shown in Fig. 4. Inset panels show the scan direction relative to the fiber orientation i.e. the orientation of the synthetic relative to the fiber direction. Left panel A synthetic aperture aligned parallel to fibers. Right panel B: synthetic aperture aligned perpendicular to fibers.

material anisotropy into the reconstruction algorithm, particularly for flaws at greater depths.

REFERENCES:

1. J. Seydel, "Ultrasonic Synthetic-Aperture Focusing Techniques in NDT," *Research Tech. Nondest. Test.*, 6, R.S. Sharpe, Ed., (Academic Press, N.Y., 1982), pp. 1-47.
2. J. Johnson, "Parameter Study of Synthetic-Aperture Focusing in Ultrasonics," *Review of Progress in QNDE*, 1, D.O. Thompson, D.E. Chimenti, Eds., (Plenum Press, N.Y., 1982), pp. 735-752.
3. S. Kramer, "Ultrasonic Weld Defect Sizing Using the Synthetic Aperture Focusing Technique," *Review of Progress in QNDE*, 8B, D.O. Thompson, D.E. Chimenti, Eds., (Plenum Press, N.Y., 1988), pp. 1995-2002.
4. R.N. Thomson, "Transverse and Longitudinal Resolution of the Synthetic Aperture Focusing Technique," *Ultrasonics*, 22, No. 1, (Butterworth, UK, Jan. 1984), pp. 9-15.

5. S.F. Burch and J.T. Burton, "Ultrasonic Synthetic Aperture Focusing using Planar Pulse-Echo Transducers," *Ultrasonics*, 22, No. 6, (Butterworth, UK, Jan. 1984), pp. 275-281.
6. S.R. Doctor, T.E. Hall, and L.D. Reid, "SAFT - The Evolution of a Signal Processing Technology for Ultrasonic Testing," *NDT International*, 19, No. 3 (Butterworth, UK, June 1986), pp. 163-167.
7. B.A. Barna and J.A. Johnson, "The Effects of Surface Mapping Corrections with Synthetic-Aperture Focusing Techniques on Ultrasonic Images," *Review of Progress in QNDE*, 1, D.O. Thompson, D.E. Chimenti, Eds., (Plenum Press, N.Y., 1982), pp. 753-760.